

R. Maingi<sup>a</sup>, M.G. Bell<sup>b</sup>, R.E. Bell<sup>b</sup>, J. Bialek<sup>c</sup>, C. Bourdelle<sup>b</sup>, C.E. Bush<sup>a</sup>, D.S. Darrow<sup>b</sup>, E.D. Fredrickson<sup>b</sup>, D.A. Gates<sup>b</sup>, M. Gilmore<sup>f</sup>, T. Gray<sup>i</sup>, T.R. Jarboe<sup>e</sup>, D.W. Johnson<sup>b</sup>, R. Kaita<sup>b</sup>, S.M. Kaye<sup>b</sup>, S. Kubota<sup>f</sup>, H.W. Kugel<sup>b</sup>, B.P. LeBlanc<sup>b</sup>, R.J. Maqueda<sup>e</sup>, D. Mastrovito<sup>b</sup>, S.S. Medley<sup>b</sup>, J.E. Menard<sup>b</sup>, D. Mueller<sup>b</sup>, B.A. Nelson<sup>g</sup>, M. Ono<sup>b</sup>, F. Paoletti<sup>c</sup>, H.K. Park<sup>b</sup>, S.F. Paul<sup>b</sup>, T. Peebles<sup>f</sup>, Y-K.M. Peng<sup>a</sup>, C.K. Phillips<sup>b</sup>, R. Raman<sup>g</sup>, A.L. Rosenberg<sup>h</sup>, A.L. Roquemore<sup>b</sup>, P.M. Ryan<sup>a</sup>, S.A. Sabbagh<sup>c</sup>, C.H. Skinner<sup>b</sup>, V.A. Soukhanovskii<sup>b</sup>, D. Stutman<sup>d</sup>, D.W. Swain<sup>a</sup>, E.J. Synakowski<sup>b</sup>, G. Taylor<sup>b</sup>, J. Wilgen<sup>a</sup>, J.R. Wilson<sup>b</sup>, G.A. Wurden<sup>e</sup>, S.J. Zweben<sup>b</sup>, and the NSTX Team

<sup>a</sup>Oak Ridge National Laboratory, Oak Ridge TN, 37831 USA

<sup>b</sup>Princeton Plasma Physics Laboratory, PO Box 451, Princeton, NJ, 08543 USA

<sup>c</sup>Columbia University, New York, NY, USA

<sup>d</sup>Johns Hopkins University, Baltimore, MD, USA

<sup>e</sup>Los Alamos National Laboratory, Los Alamos, NM, USA

<sup>f</sup>University California at Los Angeles, Los Angeles, CA USA

<sup>g</sup>University Washington, Seattle, WA, USA

<sup>h</sup>Princeton University, Princeton, NJ USA

<sup>i</sup>North Carolina State University, Raleigh, NC USA

## Introduction and Machine Description

The National Spherical Torus Experiment (NSTX) is a low aspect-ratio fusion research facility<sup>1,2</sup> ( $R=0.86\text{m}$ ,  $a=0.67\text{m}$ ,  $R/a = 1.26$ ,  $B_t = 0.6 \text{ T}$ ,  $I_p = 1.5 \text{ MA}$ ) which commenced physics operation in July 1999. A cross-section of the device is shown in Fig. 1. The solenoid inside the slender center stack provides up to 0.7 volt-seconds of inductive flux while the outer poloidal field coils control the plasma shaping and divertor configuration. Auxiliary heating is provided by a neutral beam injector (NBI), which has delivered up to 7 MW and a radio-frequency (30 MHz) antenna system which has delivered up to 6 MW to the plasma. The passive stabilizing plates above and below the outer midplane are designed to enhance magneto-hydrodynamic (MHD) stability. An important design feature is the electrical isolation between the inboard and outboard vessel segments, to permit the investigation of current initiation by coaxial helicity injection (CHI). All of the plasma facing components on the center stack divertor and passive stabilizers are clad in graphite armor. NSTX employs a conventional wall conditioning program<sup>3</sup>, which includes  $350^\circ\text{C}$  bake-out, surface boronization, and routine glow discharge cleaning.

The goal of NSTX research is to make a determination of the attractiveness of the spherical torus (ST) concept by assessing high- stability, confinement, the achievability of self-consistent high-bootstrap operation, and acceptable divertor heat flux, for pulse lengths much longer than the energy confinement time. To this end, the research is divided into several science topics: confinement and transport, stability, non-inductive current drive, and boundary physics. In addition, one element of the research plan considers integration of the various elements into operating scenarios.

## Results

Prior to the 2002 experiment campaign, the standard operating configuration for NSTX was center-stack limited discharges<sup>4</sup> which exhibited L-mode edge profiles, but many with achieved nonetheless exceptional global energy confinement. H-mode phases were obtained<sup>5</sup> in lower-single null configuration but were short-lived, due to the onset of locked tearing or external kink modes. Several important improvements were implemented between the 2001

and 2002 campaigns. These included: 1) a reduction of the intrinsic error field by realignment of the outermost poloidal field coils, 2) introduction of a higher temperature bakeout allowing all graphite tiles to reach 350°C, and 3) implementation of the capability to fuel the plasma on the inboard side from a gas injector in the center stack at the midplane. The combination of these improvements has enabled the development of routine, long-pulse (often ELM-free) H-mode discharges, an example of which is shown in Fig 2.

The remainder of this paper discusses results from the various topical areas of research with an emphasis on results obtained during the last calendar year. Additional recent overviews<sup>6</sup> of NSTX results are noted here.

### a. Confinement, Transport and Turbulence

The NSTX program on transport and turbulence aims to characterize global confinement as well as local particle transport studies via impurity injection, and energy transport studies. In general, energy confinement is often higher than the predictions extrapolated from scalings developed from conventional aspect ratio tokamaks. For example the long pulse discharge in Fig. 2 exceeded the values predicted by the commonly used ITER98pby(2) scaling<sup>7</sup> by as much as 50%. In computing the confinement time, we note the stored energy of the fast ion component, the neutral beam shine through, and the bad orbit and charge exchange beam ion losses were not taken into account. Estimates with the TRANSP code for select discharges have indicated a fast ion content between 10-20% and a beam ion loss of approximately the same magnitude. The measured confinement times are also above scalings which consider the total energy content, e.g. Fig. 2 \\* MERGEFORMAT shows that the NSTX data are more than twice the ITER89-P L-mode scaling<sup>8</sup>. An interesting facet of the NSTX data is that high energy confinement times are observed in discharges with either L-mode and H-mode profiles. L-mode discharges often show a secular increase in stored energy and energy confinement until an H-mode transition or until the discharge is terminated by the volt-second limit from the solenoid. The cause of the excellent confinement with the L-mode edge profiles is under investigation.

The local transport properties have been studied through particle transport<sup>9</sup> in which trace quantities of neon have been injected and the evolution of the emission in the ultra-soft X-ray bands has been followed. The densities of the high charge-state of neon are inferred (Fig. 3) and compared with simulations with the MIST code<sup>10</sup>. From amongst an ensemble of model profiles, the neon diffusion coefficient profile which best matches the data has a discontinuity at  $r/a \sim 0.6$ . Inside that region the diffusion coefficient falls to about twice the value predicted by the NCLASS neoclassical transport code<sup>11</sup>.

Local energy transport coefficients have been difficult to derive, however. In many NBI-heated NSTX discharges, the ion temperature is well above<sup>12</sup> the electron temperature, even though  $\sim 2/3$  of the NBI heating is computed to go to the electrons. This high  $T_i/T_e$  ratio is often inexplicable within the classical collisional framework. Several mechanisms to transfer additional energy to the ions have been hypothesized, and experiments to investigate these possibilities are ongoing. In the near term, however, quantitative momentum transport analysis will augment the particle and energy transport studies because momentum diffusivities are believed to be related to ion thermal diffusivities.

The connection between turbulence and transport is being investigated via gas puff imaging<sup>13</sup> at the edge and correlation reflectometry in the core. Small quantities of helium are puffed into the edge plasma of deuterium-fueled discharges and the helium line emission is imaged with a fast framing visible camera along a line of sight roughly parallel to the magnetic field lines in the edge. The helium emission has higher fluctuation amplitude and

shows more pronounced turbulent structures in L-mode plasmas compared with H-mode plasmas. The results are being compared with the BOUT 3-D turbulence code<sup>14</sup>. Correlation reflectometry was recently implemented; first results<sup>15</sup> show that the turbulence decorrelation length decreases with increasing toroidal field.

In 2001, the H-mode power threshold was measured<sup>5</sup> in NSTX to be  $\sim 1$  MW total loss power for  $I_p=900$  kA,  $B_t=0.45$  T, line-average density  $\sim 2 \times 10^{19} \text{ m}^{-3}$ , in a lower-single null diverted configuration with the ion grad-B drift toward the X-point. This value is  $\sim 17$  times the prediction of the EPS-97 scaling<sup>16</sup> for conventional aspect ratio tokamaks, and  $\sim 4$  times higher than more recent scalings<sup>17</sup>. In 2002, the power threshold was measured to be 30% lower at the same  $B_t$  and  $I_p=600$  kA. We are investigating whether these two datasets<sup>17</sup> imply an  $I_p$  dependence or a systematic decline of the power threshold as wall conditions have improved.

### b. Magnetohydrodynamic Stability

Studies of limits and associated instabilities comprise an essential part of NSTX research. We have examined the scaling of the maximum  $\tau = \langle p \rangle / (B_{t0}^2 / 2\mu_0)$ , where  $B_{t0}$  is the vacuum toroidal field at the plasma geometric center, with the normalized current  $I_p/aB_t$  (Fig. 4). To date, we have attained  $\tau = \sim 34\%$  and  $N = \sqrt{(I_p/aB_t)} \sim 6.5 \text{ } \% \cdot \text{m} \cdot \text{T/MA}$ . Stability calculations<sup>6</sup> without including the effects of a conducting shell indicate that this plasma would be MHD unstable. The presence of the passive stabilizers and the observed high toroidal rotation rates are thought to stabilize the predicted MHD activity. The highest  $N$  discharges are, in fact, approximately half-way between the computed no-wall and ideal-wall stability boundaries. When rotation slows down sufficiently, a non-rotating resistive wall mode is observed<sup>4</sup> and causes a collapse of plasma confinement. In other cases,  $\tau$  saturates as a magnetic island precursor is observed prior to the onset of a locked mode. Preliminary analysis<sup>6</sup> indicated that the MHD activity had the characteristics of a neoclassical tearing mode (NTM). In 2001, these MHD modes restricted NSTX to  $\rho \sim 0.5$  when  $q(0) (= q_{min})$ , as determined by EFIT<sup>18</sup> from the external magnetic data, was below 1.5; in 2002,  $\rho \sim 1.4$  have been achieved without the signature of these modes for extended periods ( $>0.2\text{s}$ ), in plasmas with mildly reversed shear and  $q_{min} > 2$ .

We have also examined the dependence of the  $N$  limit on the plasma internal inductance, Fig. 5 shows that NSTX  $N$  data are bounded by  $\sim 10 \times \ell_i$ . For reference, the conceptual design point for NSTX was  $N \sim 8$  at  $\ell_i \sim 0.2-0.3$ . One reason that NSTX has been able to extend to high  $N/\ell_i$  is the low pressure peaking factors  $\sim 2$  produced in H-modes plasmas. NSTX data show (see Fig. 5) a dramatic increase in maximum  $N$  as pressure peaking is reduced, similar to reports from tokamaks<sup>19</sup>.

### c. Non-inductive current generation and sustainment

Non-inductive current initiation and drive are crucial elements of NSTX research, owing to the limited volt-second capability of the central solenoid in the ST. In the area of discharge initiation, CHI is being studied in NSTX. Details of the implementation of CHI in NSTX are given in a recent paper<sup>20</sup>. In brief, the inner vacuum vessel is biased with respect to the outer one to initiate a discharge between electrodes which carries a poloidal current. In the presence of a toroidal magnetic field, toroidal current develops. The  $J \times B$  force causes the plasma to grow into the main chamber from the injector region. It is expected, and previous experiments in smaller devices have shown, that the resulting plasma is unstable and that MHD activity and hypothesized magnetic reconnection cause the toroidal current to form closed, nested flux surfaces.

CHI discharges with toroidal current up to 400 kA have been produced in NSTX (Fig. 6) An n=1 MHD mode was observed during the high current phase, and oscillations in the toroidal current are possibly signatures of magnetic reconnections. In the high current CHI discharges, soft-X-ray emission from the center is observed, implying a core temperature of 30-40 eV and suggestive of a small region of closed flux surfaces.

An multiple-element antenna launching radio-frequency waves at a high multiple (10 – 15) of the cyclotron frequency and parallel wave number  $k_{\parallel} = \pm(7 - 14) \text{ m}^{-1}$  is used for heating and current drive studies. A rapid increase in electron temperature after RF turn-on with  $k_{\parallel} = 14 \text{ m}^{-1}$  demonstrates that the system successfully heats the plasma (Fig. 7). As expected the central electron temperature exceeds the central ion temperature because the RF damps mainly on the electrons. Preliminary comparisons between current drive and anti-current drive phasings with  $k_{\parallel} = 7 \text{ m}^{-1}$  have shown a transient drop in loop voltage required to maintain constant plasma current (Fig. 8). In this experiment, the RF power was adjusted to match the electron temperature profiles; less power was required in the anti-current drive phasing than the co-current drive phasing. Even considering changes in the plasma internal inductance, analysis of this difference in loop voltage indicates that some non-inductive current was produced. The difference in loop voltage was transient, and as the internal inductance further evolved, the loop voltage became similar for both phasings. Future experiments will focus on extension of the phasing comparison to higher RF power and longer duration.

#### d. Boundary physics

Boundary physics research in NSTX focuses on power and particle balance, with limited but increasing emphasis on boundary transport. Use of a divertor configuration is required at present for H-mode access, but it leads to high peak heat flux on the target plates. Previously a peak heat flux of  $6 \text{ MWm}^{-2}$  was reported<sup>21</sup> in L-mode lower-single null discharges with heating power  $\sim 5 - 6 \text{ MW}$ . More recently, the peak heat flux in lower-single null H-mode plasmas with  $4.5 \text{ MW}$  of heating power has reached  $10 \text{ MWm}^{-2}$ , with a full-width half-max of 2 cm at the target (Fig. 9). A tile temperature increase of  $300 \text{ }^{\circ}\text{C}$  was measured during the first 0.2 s after the divertor was established during this discharge. Extrapolation of the temperature rise, assuming an increase  $\sim (\text{time})^{1/2}$  with constant peak heat flux, yields a tile temperature in excess of the  $1200 \text{ }^{\circ}\text{C}$  limit after  $\sim 3 \text{ s}$ . While this limitation should not impact the NSTX near-term program, investigating pulse lengths of several energy confinement times, it could impede progress on the long-term research goal of investigating pulse lengths of several current skin times, i.e. up to 5 s. As pulse lengths are increased in NSTX, the emphasis in boundary physics research will be placed on using double-nulls, radiative divertor/mantle solutions, and X-point sweeping.

Particle balance analysis<sup>22</sup> has shown gas fueling efficiencies between 5% and 20%, independent of the poloidal location of the gas injector. Despite this observation, access to H-mode is more reproducible with high-field side fueling (i.e. from the injector on the center column), as compared with low-field side fueling alone. The successful development of routine, long-pulse H-mode discharges has highlighted the need for density control. The rate of increase in the particle content is 2-3 times the particle source rate from NBI during the ELM-free phase for the discharge in Fig. 2. Although some portion of this density rise is due to high-field side gas injection which fuels for the entire discharge duration, other H-mode discharges without any explicit gas fueling exhibit a similar density rise rate. In-vessel density control techniques such as cryopumping or a liquid lithium divertor module are being considered as upgrades over the next few years.

An integral part of the boundary physics program is the development and refinement of wall conditioning techniques, mentioned in the introduction. Direct fueling of deuterium discharges with deuterated trimethylboron (the same material used during glow discharge boronization) was recently tested<sup>23</sup>. Fiducial deuterium-fueled discharges before and after the fueling sequence showed a rise in the central electron temperature and a drop in the core radiated power, but the edge impurity light was largely unaffected. Future experiments will test the duration of the effect.

#### e. Integrated scenario development

Scenario development experiments have two main goals: discharges combining high confinement, and long-duration discharges. Progress toward the first goal was made by combining the high triangularity (~0.8), double-null discharge shape used for high  $\beta$  studies with H-mode operation. Fig. 10 shows a discharge which maintained  $\tau_{\text{E}}=16\%$  and a minimum  $E \sim 80\text{ms}$  for  $\sim 80\text{-}100\text{ms}$  during the ELM-free H-mode phase. Note that maximum  $E \sim 120\text{ms}$  occurs just after the L-H transition and is largely related to the increase in the  $dW/dt$  term. Note also that most of the build-up in stored energy occurred during the L-mode phase, and that after the H-mode transition the stored energy increased by only  $\sim 15\%$ .

Long ELM-free H-modes in lower-single null configuration provided the lowest volt-second consumption and longest pulse length, approaching  $\sim 1\text{ s}$ , as seen in Fig 11. During the NBI-heated H-mode phase, loop voltage dropped to  $\sim 0.1\text{ volts}$  as  $\beta_p$  approached 1.2. In a similar discharge, the bootstrap current was estimated to be 40%. We note that the high performance phase is typically terminated between 500-700ms. The cause of termination is not yet understood.

### **Summary and Conclusions:**

The research program in NSTX is making excellent progress toward a broad assessment of the attractiveness of the ST concept. Routine H-mode operation has been enabled by recent machine upgrades. Confinement is generally above conventional aspect ratio tokamak scalings, and particle transport in the core has approached neoclassical in some conditions. Discharges above the ideal no-wall stability limits have been obtained, with maximum  $\tau_{\text{E}} \sim 34\%$  and  $N \sim 6.5$ . Current initiation via CHI has produced 400 kA discharges with some evidence for the formation of closed flux surfaces. Indications of non-inductive current drive with the RF heating have been obtained for limited duration. The measured heat flux to the divertor is acceptable for present pulse duration; future research will focus on mitigation techniques for long pulses and also on density control. Combination of results from these science elements has enabled the development of both simultaneously high  $\tau_{\text{E}}$  and  $E$  and long pulse discharges.

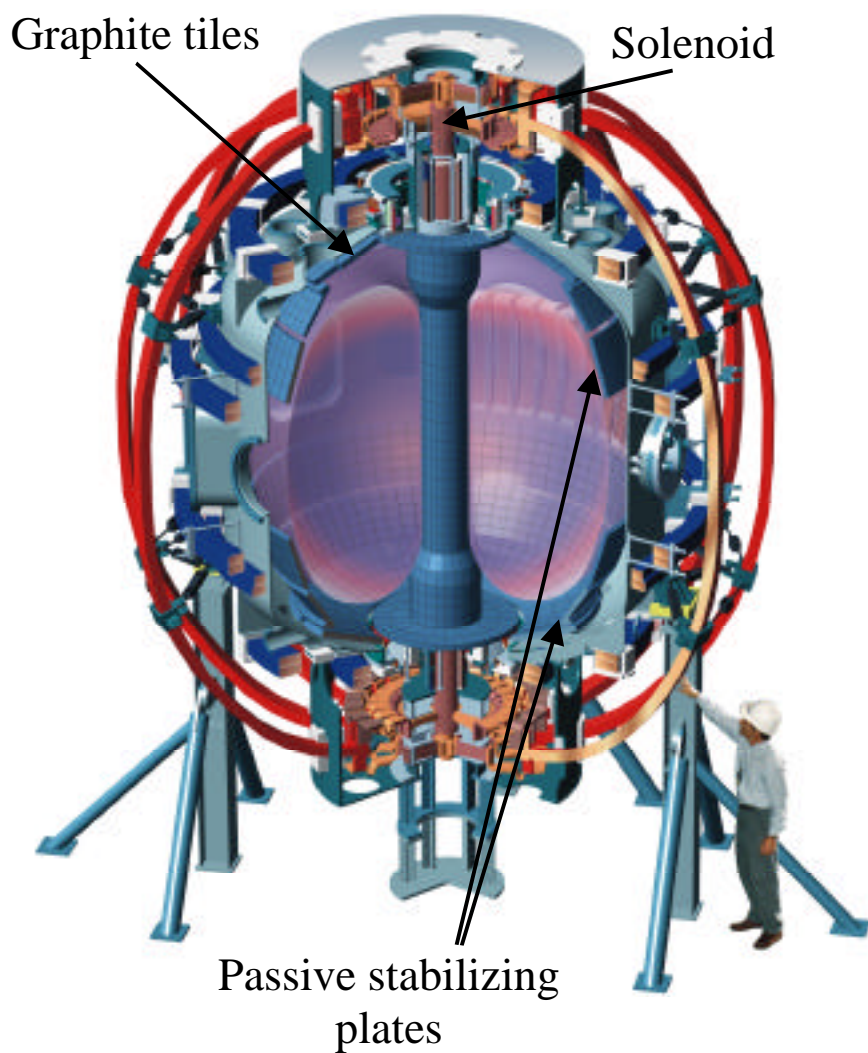
### **Acknowledgements:**

This research was supported by the U. S. Dept. of Energy under contracts DE-AC05-00OR22725, DE-AC02-76CH03073, DE-AC04-94AL85000, W-7405-ENG-36, W-7405-ENG-48 and grants DE-FG02-99ER54524 and DE-FG02-99ER54523. We gratefully acknowledge the contribution of the NSTX technical staff and neutral beam operations staff.

### **Figure Captions:**

1. Cross-section of the NSTX device.
2. Time dependence of several quantities for a routine H-mode ( discharge #108728). Panel 5 shows the NSTX confinement time relative to the ITER89P scaling(solid) and the ITER98pby(2) scaling (dashed)
3. Inferred Neon distribution distributions for  $Ne^{8,9,10}$  lines (charge states +7, +8, +9) from ultra-soft X-ray emission profiles. Panel 3 shows the diffusion coefficient used in the MIST simulation which best matches the charge state distributions, compared with a neoclassical transport calculation from the NCLASS code.
4. Database plot of  $\tau$  vs  $I_p/(aB_{t0})$ , showing the data are bound by a line with slope  $\sim 6.0-6.5$ . Discharges are divided into experimental data in 2002 vs previous years' results.
5. Database plots of  $\tau_N$  vs  $\ell_i$  and pressure peaking factor. Data from 2002 with 'partial kinetic' EFITs are shown<sup>4</sup> in red, whereas data from previous years with magnetics-only EFITs are shown in gray. The solid line shows the 'tokamak' limit of  $4 \times \ell_i$ .
6. Time traces for a high current CHI discharge. MHD activity ( $n=1$ ) was observed during the high current phase during times shown by arrow in panel 2.
7. Time traces and profiles showing evidence of electron heating during the application of HHFW. Central  $T_e$  was higher than  $T_i$ , as expected.
8. Time traces comparing loop voltage for HHFW discharges with co-current drive and counter-current drive phasings. The electron temperature profiles were well matched, and the electron density profiles were similar to within 15%.
9. Heat flux profile for a lower-single null ELM-free H-mode discharge. The equilibrium is shown in the inset.
10. Time traces of double-null discharge with simultaneously high  $\tau$  and  $T_e$ . The H-mode transition is indicated by the dashed line.
11. Time traces of lower-single null ELM\_free H-mode discharge which achieved pulse length  $\sim 1$  sec. The time of the H-mode transition is shown by the dashed line.

Fig. 1



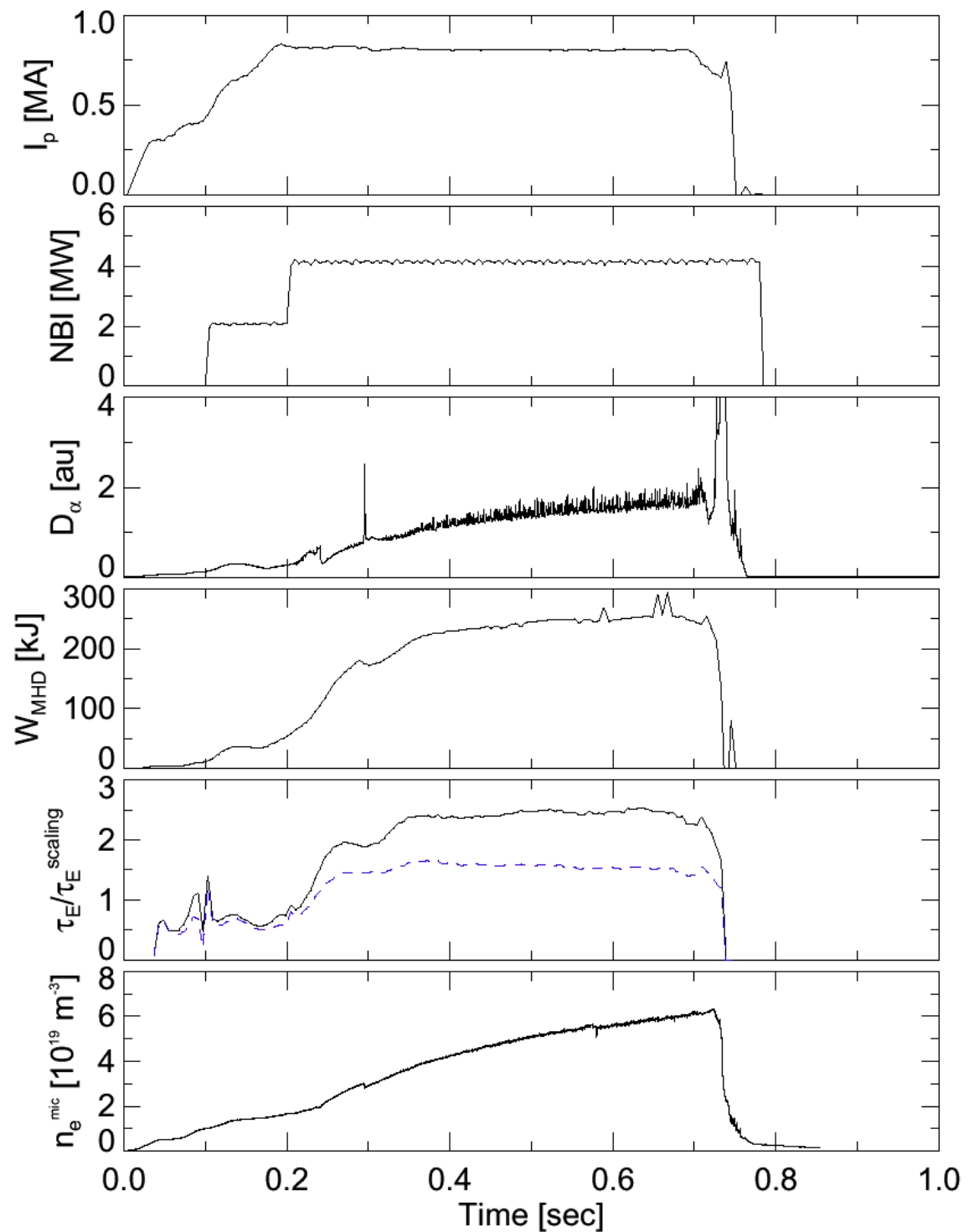
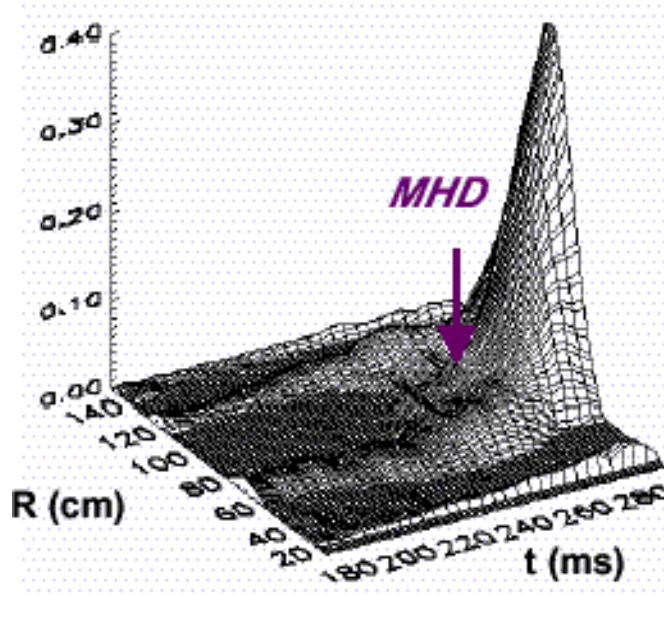


Fig. 2

**$E > 1.4 \text{ keV}$**   
**( $\text{Ne}^{10+}$ )**



**$E > 0.6 \text{ keV}$**   
**( $\text{Ne}^{8,9+}$ )**

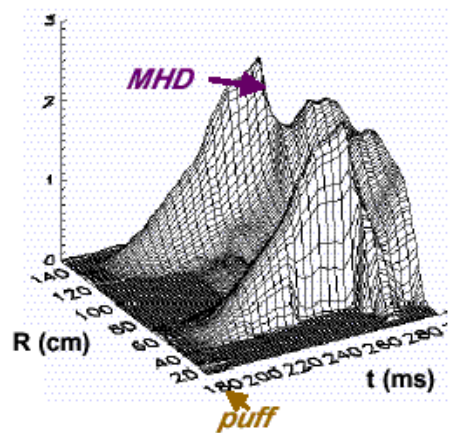


Fig. 3

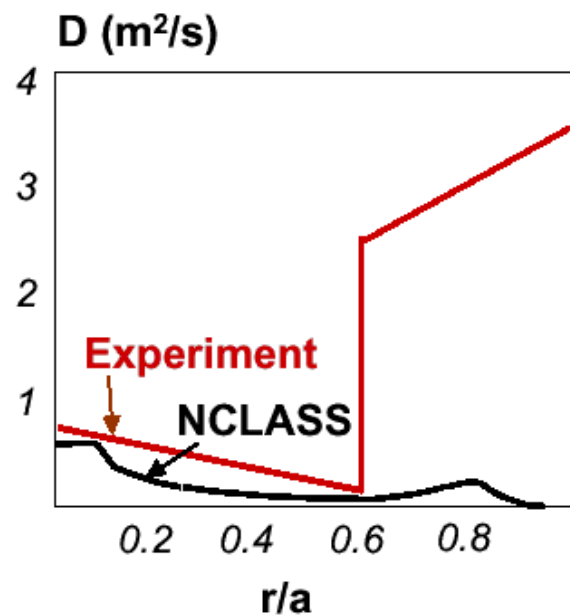


Fig. 4

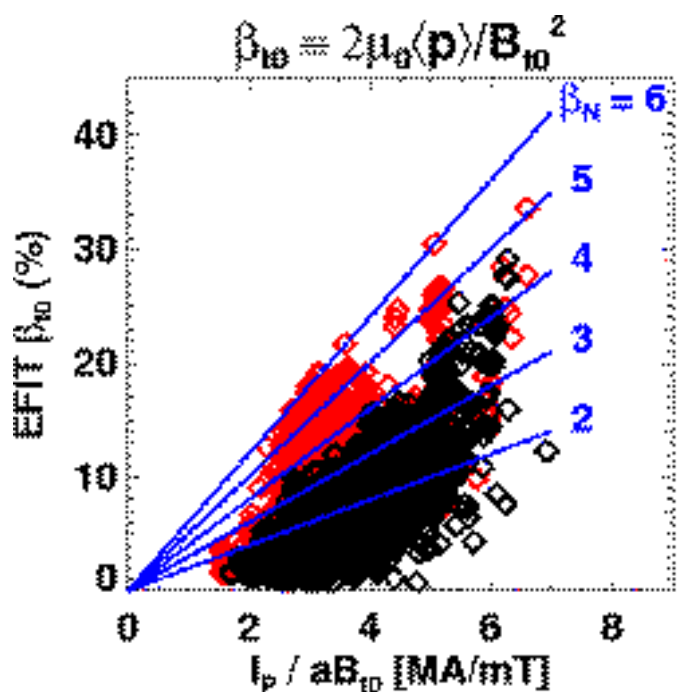


Fig. 5a

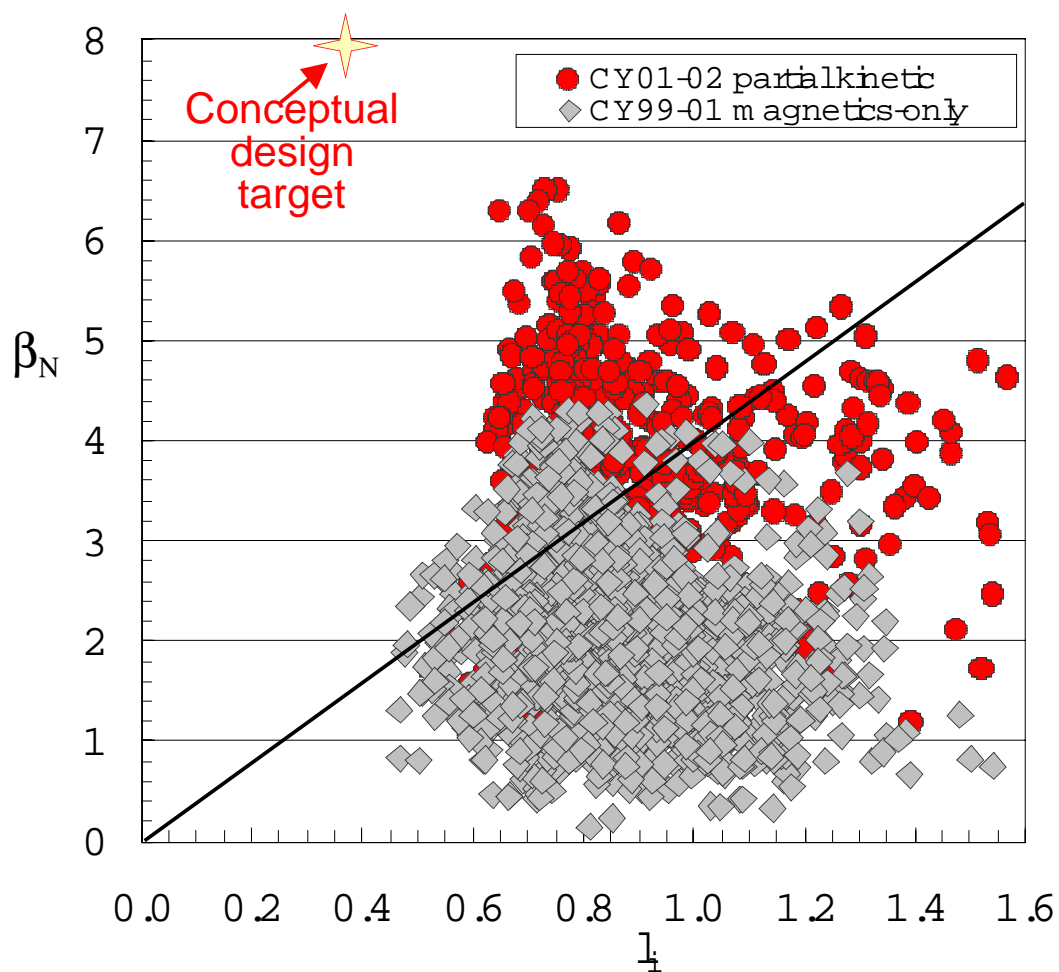


Fig. 5b

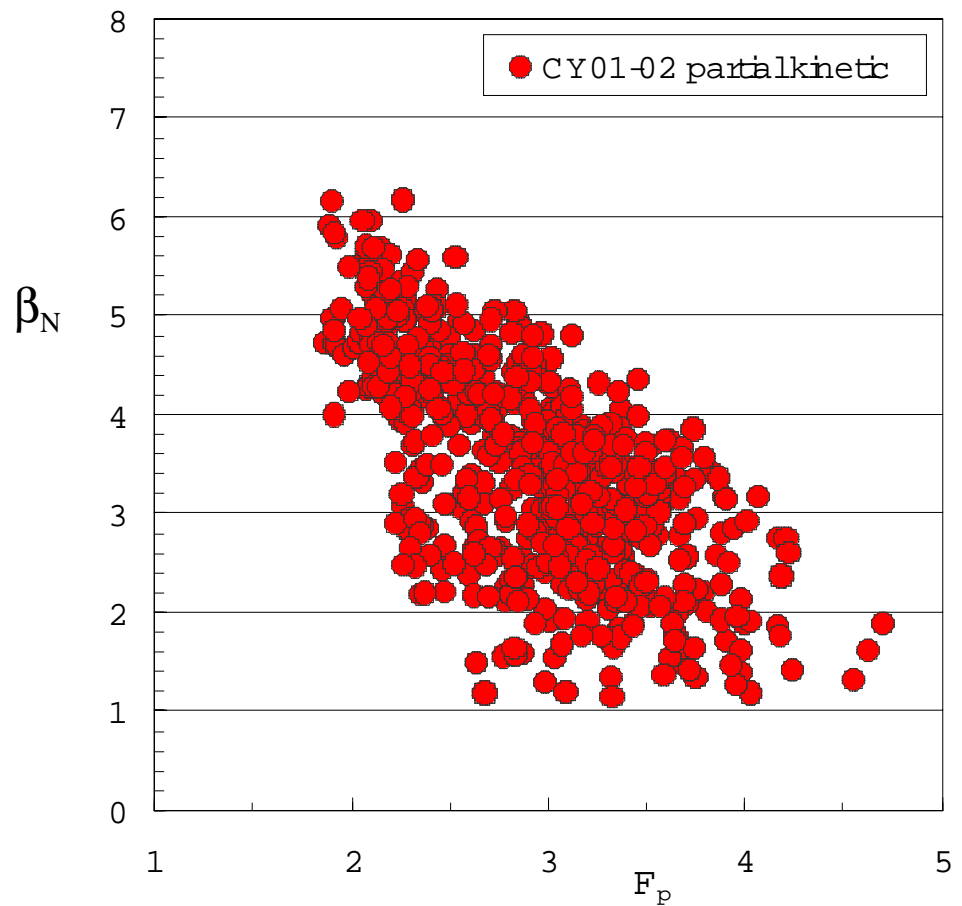


Fig. 6

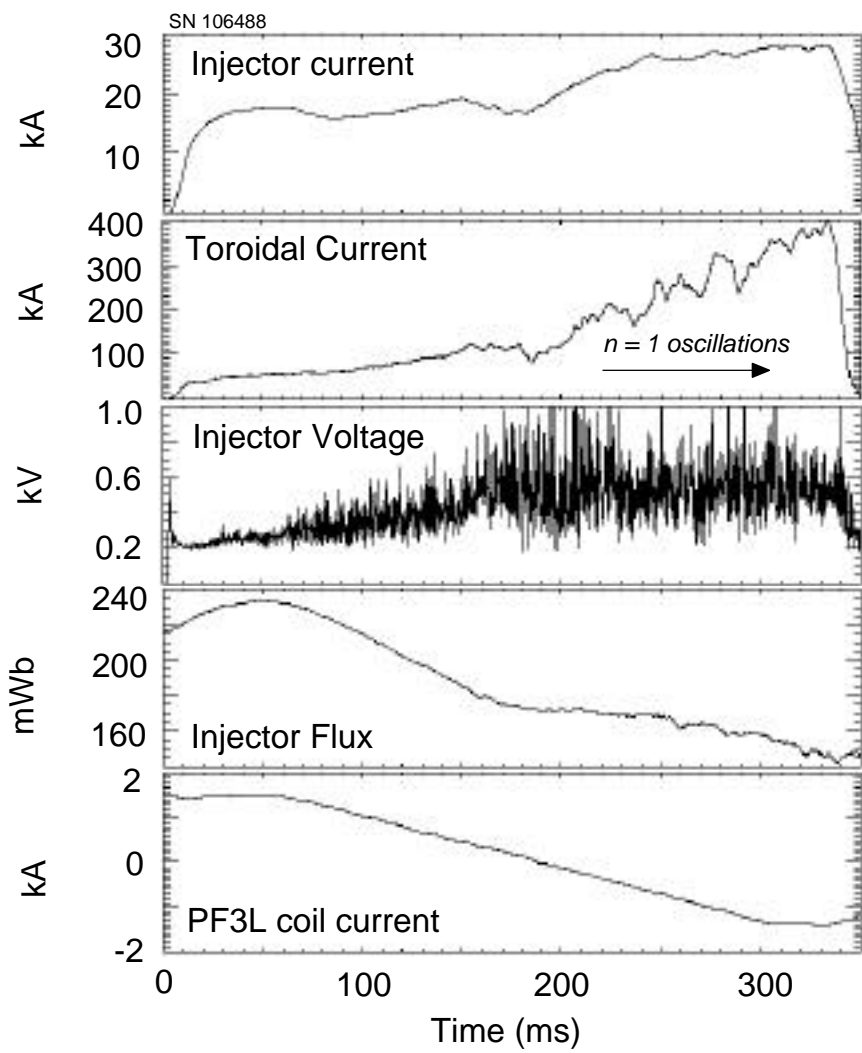


Fig. 7

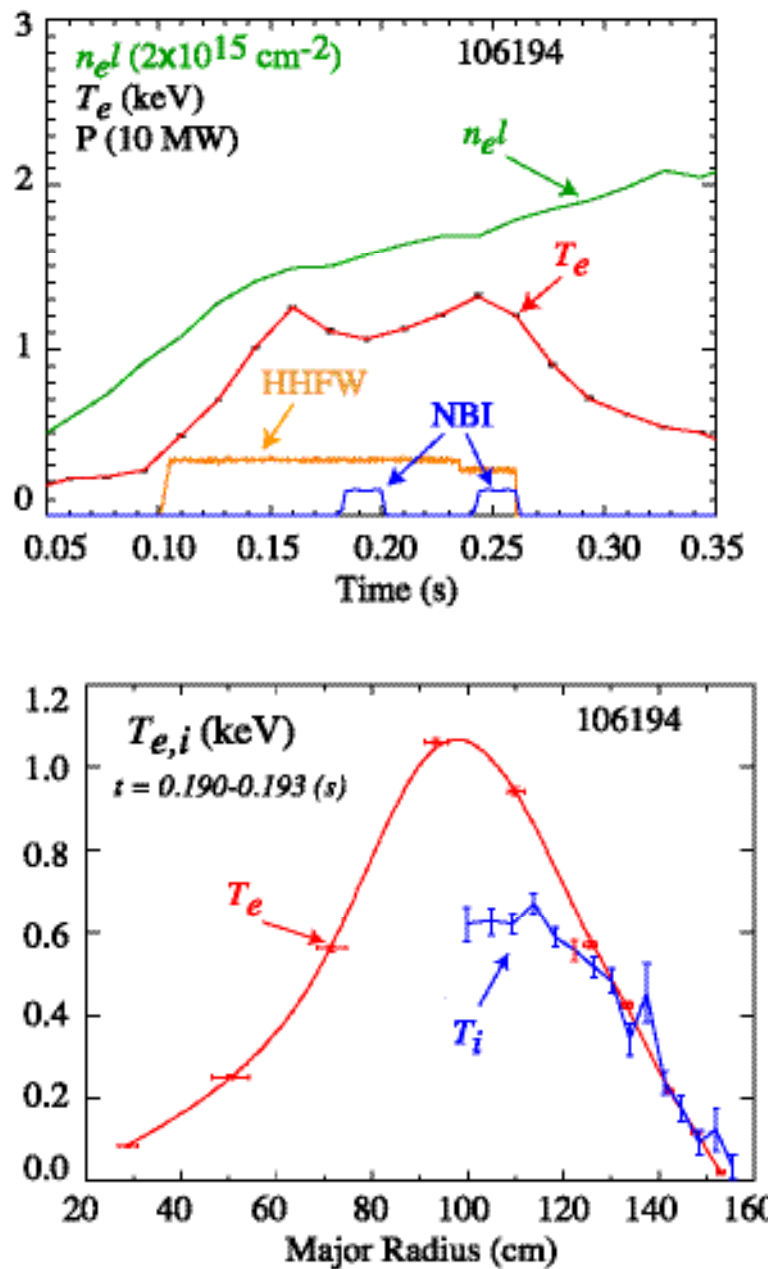


Fig. 8

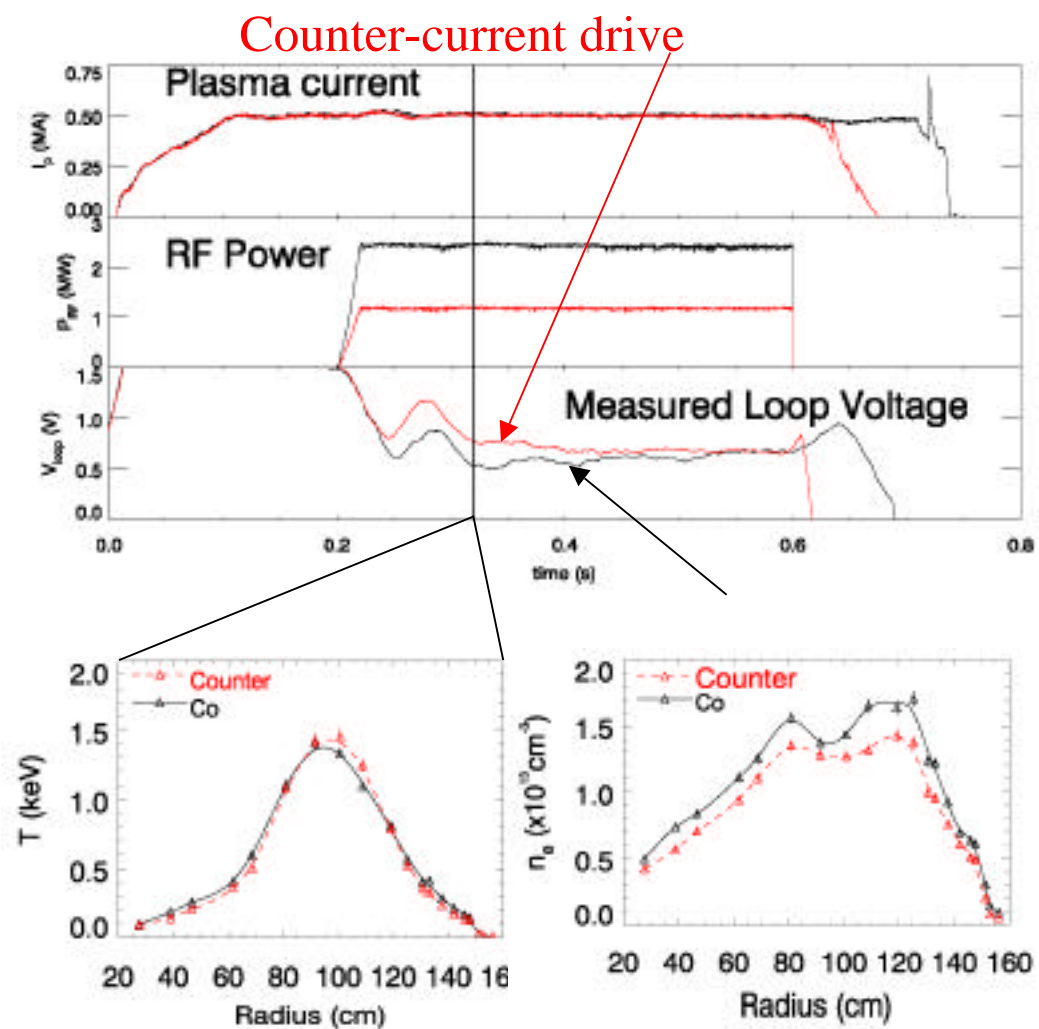
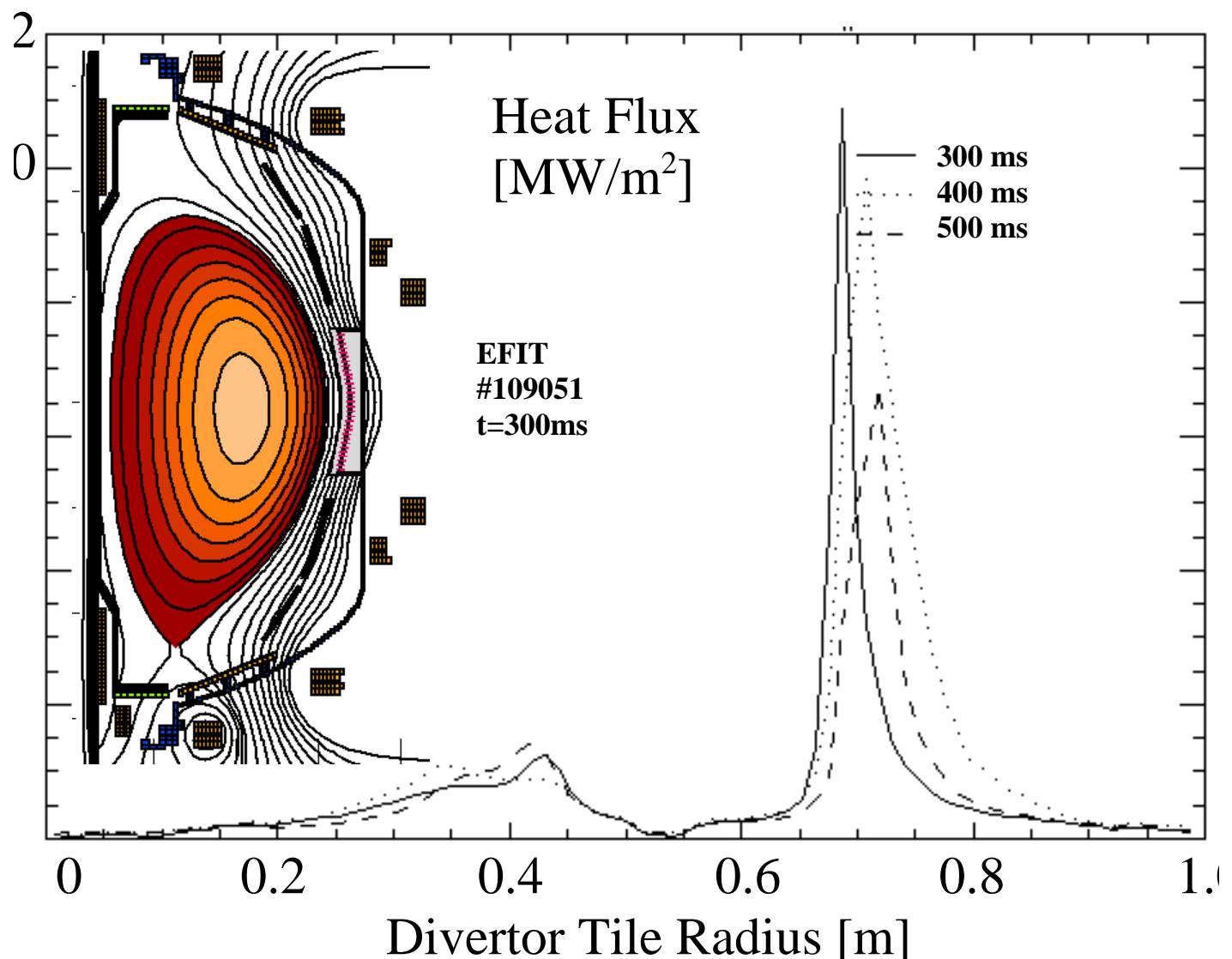


Fig. 9



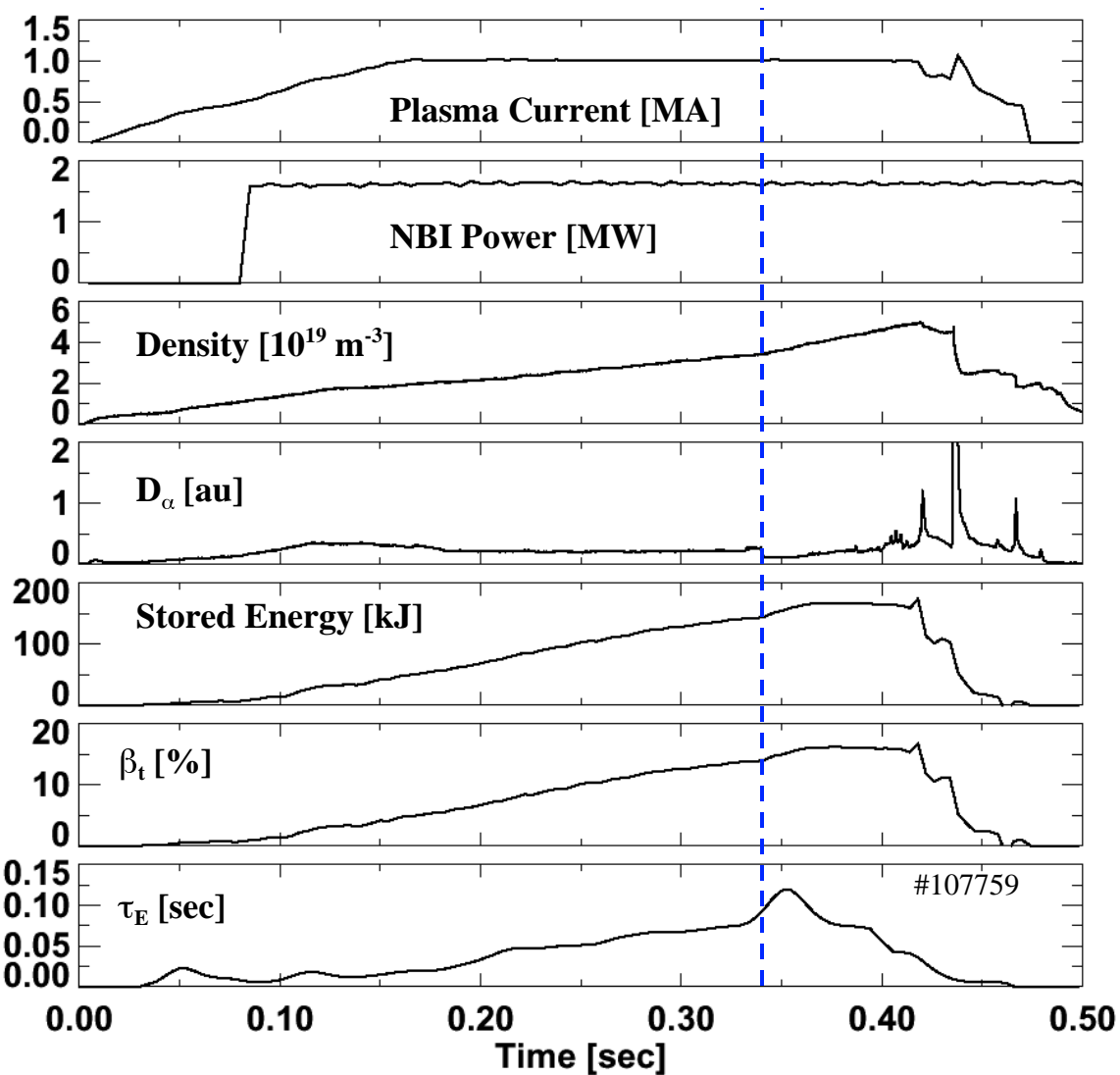


Fig. 10

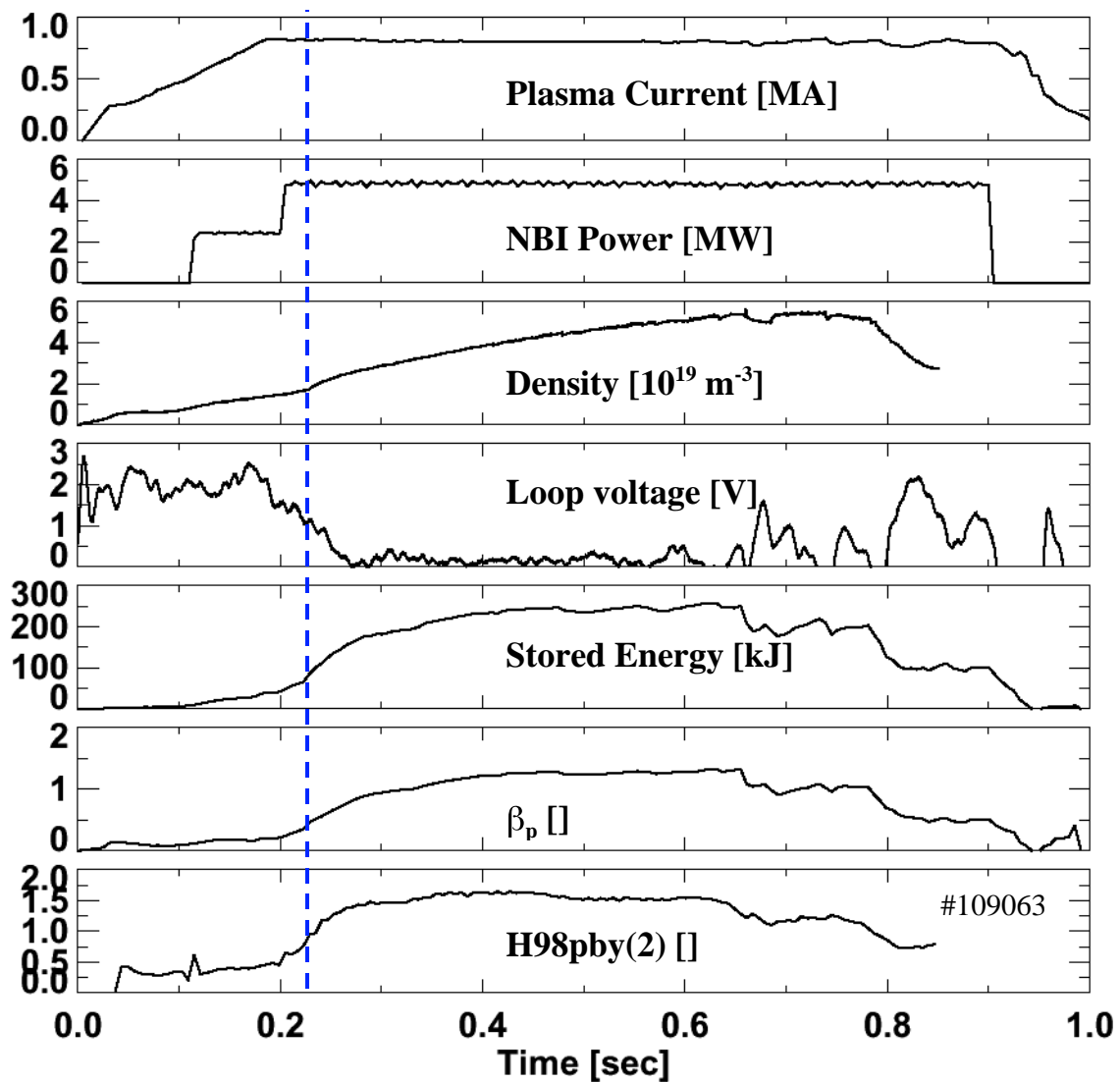


Fig. 11

## References

---

- <sup>1</sup> M. Ono et. al., *Phys. Plasmas* **4** (1997) 799.
- <sup>2</sup> C. Neumeyer et. al., *Fusion Eng. and Design* **54** (2001) 275.
- <sup>3</sup> H.W. Kugel et. al., *J. Nucl. Mater.* **290-293** (2001) 1185.
- <sup>4</sup> S.A. Sabbagh, et. al., *Phys. Plasmas* **9** (2002) 2085
- <sup>5</sup> R. Maingi, et. al., *Phys. Rev. Letts.* Vol. **88**, no. 3 (21 Jan 2002) article #035003; C.E. Bush, et. al., to appear in Proc. of 8<sup>th</sup> Technical Meeting on H-mode Physics and Transport Barriers, Toki Japan, Sept. 5-7, 2001.
- <sup>6</sup> D. Gates, et. al., to appear in Proc. of Euro. Physical Society Meeting on Controlled Fusion and Plasma Physics, Montreux, SZ, June 17-22, 2002; D. Mueller, et. al., to appear in Proc. 29<sup>th</sup> International Conference on Plasma Science, Alberta, CA, June 17-22, 2002.
- <sup>7</sup> Authors of ITER physics basis, *Nucl. Fusion* **39** (1999) 2137.
- <sup>8</sup> P.N. Yushmanov, et. al., *Nucl. Fusion* **30** (1990) 1999.
- <sup>9</sup> D. Stutman, et. al., Proc. 29<sup>th</sup> Euro. Physical Society Meeting on Controlled Fusion and Plasma Physics, Montreux, SZ, June 17-22, 2002.
- <sup>10</sup> R.A. Hulse, *Nuclear Technology/Science* **3** (1983) 259.
- <sup>11</sup> W.A. Houlberg, et. al., *Phys. Plasma* **4** (1997) 3230.
- <sup>12</sup> D.A. Gates, et. al., *Phys. Rev. Letts.*, vol. **87**, no. 20 (12 Nov. 2001) Article #205003.
- <sup>13</sup> S. Zweben, Proc. 29<sup>th</sup> Euro. Physical Society Meeting on Controlled Fusion and Plasma Physics, Montreux, SZ, June 17-22, 2002, R. Maqueda, et. al., Proc. 14<sup>th</sup> High Temp. Plasma Diagnostics Conf., Madison, WI, July 8-11, 2002.
- <sup>14</sup> X. Xu, el. al., *Phys. Plasma* **7** (2000) 1955.
- <sup>15</sup> M.A. Gilmore, private communication, 2002.
- <sup>16</sup> J. A. Snipes, Proc. 24<sup>th</sup> Euro. Physical Society Meeting on Controlled Fusion and Plasma Physics, Berchtesgaden, Germany, Pt. III, P. 961.
- <sup>17</sup> C.E. Bush, et. al., Proc. 29<sup>th</sup> Euro. Physical Society Meeting on Controlled Fusion and Plasma Physics, Montreux, SZ, June 17-22, 2002.
- <sup>18</sup> L.L. Lao, et. al., *Nucl. Fusion* **25** (1985) 1611.
- <sup>19</sup> S.A. Sabbagh, et. al., Proc. of 1996 Fusion Energy Conference (IAEA, Vienna, 1997) 921; E.A. Lazarus, *ibid*, p.199.
- <sup>20</sup> R.Raman,et. al., *Nucl. Fusion* **41** (2001) 1081.
- <sup>21</sup> R. Maingi, et. al., presented at the 15<sup>th</sup> International Conference on Plasma Surface Interactions, May 27-31, 2002 Gifu, Japan, to be published in *J. Nucl. Mater.*
- <sup>22</sup> V. Soukhanovskii, et. al., presented at the 15<sup>th</sup> International Conference on Plasma Surface Interactions, May 27-31, 2002, Gifu, Japan, to be published in *J. Nucl. Mater.*
- <sup>23</sup> H.W. Kugel, et. al., presented at the 15<sup>th</sup> International Conference on Plasma Surface Interactions, May 27-31, 2002, Gifu, Japan, to be published in *J. Nucl. Mater.*

R. Maingi, et. al., Invited talk presented at the 11<sup>th</sup> International Conference on Plasma, Sydney, Australia, July 15-19, 2002.